Pergamon

*Int. J. Heat Mass Transfer.* Vol. 37, No. 13, pp. 1817–1828, 1994

0017 9310/94 $7.00+0.00

0017–9310(94)E0073–4

# Effect of molecular diffusivity on point source diffusion in the center of a numerically simulated turbulent channel flow

K. KONTOMARIS† and T. J. HANRATTY‡

Department of Chemical Engineering, University of Illinois, Urbana, IL 61801, U.S.A.

(*Received* 7 *June* 1993 *and in final form* 23 *February* 1994)

**Abstract**—Molecules of a substance (or thermal markers) in a turbulent flow escape from the fluid particles in which they are released because of their molecular diffusivity. The consequences of this phenomenon on the effectiveness of turbulence to disperse a foreign substance are explored by using a Direct Numerical Simulation (DNS) of flow in a channel. Trajectories of molecules of different Schmidt (or Prandtl) numbers originating in the center of the channel are computed and property autocorrelations and other single-particle Lagrangian statistics are reported and discussed.

## 1. INTRODUCTION

MOLECULAR diffusion can cause thermal or molecular markers to escape from fluid particles, so as to decrease the effectiveness of turbulent motions in dispersing heat or mass. When the molecular diffusion coefficient is of the same order as the eddy diffusivity or larger (as, for example, in the case of liquid metal heat transfer) the effects of molecular diffusivity cannot be neglected.

This paper presents the results of a computer study of the effect of molecular diffusion on turbulent diffusion from a point source located at the center of a channel, where the flow is nearly homogeneous. The pseudospectral code of Lyons *et al.* [1] that simulates low Reynolds number turbulent flow in a two-dimensional channel is employed. The fluid particle tracking algorithm of Kontomaris *et al.* [2] is extended to trace property particles which contain either molecules of kinetic energy higher than that of the surrounding fluid (in the case of thermal markers) or molecules of a foreign species. This is accomplished by superimposing a three-dimensional random walk on the convective motion of the particles. The step size of the random walk is determined by the magnitude of the diffusivity (or equivalently the Prandtl or Schmidt number) of the property particles. By simulating the flow and the molecular diffusion process from first principles without resorting to any questionable assumptions, new accurate "data" are obtained about the interaction of molecular and turbulent diffusion.

A theoretical analysis for the effect of molecular diffusion on turbulent diffusion for small diffusion times was presented by Saffman [3, 4], who treated the idealized case of dispersion of a dynamically passive substance from a point source in a stationary, homogeneous and isotropic turbulent velocity field. He generalized Taylor's [5] Lagrangian formulation of the turbulent diffusion problem, by introducing the concept of a "substance or property autocorrelation" in order to allow for molecular effects. This correlation differs from the well-known Lagrangian autocorrelation in that it correlates fluid velocity components along the trajectories of property particles, and not of fluid particles. Since a marker can leak out of a fluid particle because of random molecular motion, the property autocorrelation is not purely a property of the turbulence, but depends also on molecular diffusivity.

For long times after release no precise calculation of molecular effects is available. A few intuitive solutions, however, have been proposed ([3, 4], Hinze [6]). Recently Kontomaris and Hanratty [7] used an iterative procedure, for calculating the effect of molecular diffusion on the property autocorrelation in isotropic turbulence for all times, which is based on the independence hypothesis of Corrsin [8, 9]. Their approach gives results which are consistent with those presented by Saffman but less restrictive. They also summarize recent related work by Phythian and Curtis [10], Drummond [11], Drummond *et al.* [12] and Sawford and Hunt [13]. A primary goal of the present paper is to provide detailed data for a practical flow so that the validity of the underlying assumptions and the range of applicability of such idealized theories could be assessed. A thorough Eulerian characterization of the flow at identical conditions has been documented by Lyons *et al.* [1].

The computer experiments in this paper differ from laboratory experiments in an important way. Since the contaminant cloud can be "frozen" and measured

†Currently with DuPont Central Research, Experimental Station, P. O. Box 80304, Wilmington, DE 19880, U.S.A.

‡To whom correspondence should be addressed.

## NOMENCLATURE

| | |
|---|---|
| $\bar{C}$ | mean volumetric concentration |
| $\bar{C}_{max}$ | maximum concentration at the center of the channel |
| $\mathbf{D}$ | molecular diffusivity |
| $D_i$ | total dispersion in the $i$th direction |
| $f_i, f_{f,i}$ | inhomogeneity factors, equation (11) |
| $H$ | channel half-width |
| $L^*$ | characteristic wall length scale |
| $L_x, L_z$ | periodicity lengths and dimensions of the computational box in the streamwise and spanwise directions |
| $p$ | probability density function of particle displacements, equation (20) |
| $P$ | probability |
| $P^*$ | characteristic wall pressure scale |
| $Pr$ | Prandtl number |
| $R$ | correlation coefficient as a measure of goodness of fit (Table 2) |
| $R_{f,i}$ | Lagrangian autocorrelation for fluid particles |
| $R_i$ | property autocorrelation, equation (2) |
| $s$ | time delay |
| $t$ | time |
| $T^*$ | characteristic wall time scale |
| $t_0$ | time of particle release |
| $\mathbf{U}$ | total Eulerian velocity |
| $u^*$ | friction velocity |
| $u_i$ | $i$th component of the fluctuating Eulerian velocity |
| $\mathbf{U}_c$ | Eulerian mean velocity at the channel center |
| $u_{rms,i}$ | $i$th component of the Eulerian RMS velocity |
| $\mathbf{V}$ | total Lagrangian velocity |
| $\langle \mathbf{V} \rangle$ | mean Lagrangian velocity |
| $v_i$ | $i$th component of the fluctuating Lagrangian velocity |
| $v_{rms,i}$ | $i$th component of the Lagrangian RMS velocity |
| $\mathbf{W}$ | three, independent standard Gaussian random numbers |
| $\mathbf{x}$ | Eulerian space coordinates |
| $\mathbf{X}$ | instantaneous Lagrangian coordinates (i.e. marker position) |
| $\mathbf{x}_0$ | marker location at the time of release |
| $\mathbf{Y}$ | total particle displacement |
| $\langle \mathbf{Y} \rangle$ | mean particle displacement |
| $\mathbf{Y}'$ | particle displacement fluctuations. |

Greek symbols

| | |
|---|---|
| $\Delta t_{tr}$ | time step for discretization of the particle tracking equation |
| $\Delta \mathbf{X}$ | total instantaneous particle displacement |
| $\Delta \mathbf{X}_h$ | hydrodynamic component of total particle displacement |
| $\Delta \mathbf{X}_m$ | molecular component of total particle displacement |
| $\Delta x_{pr}, \Delta z_{pr}$ | initial spacings between particles at time of release |
| $\Delta y_2$ | bin width for calculation of particle displacement probability density direction, equations (20) and (21) |
| $\Lambda_i$ | characteristic length scale in non-istropic extension of Saffman's theory equations (8) and (11) |
| $\lambda_{ij}$ | Eulerian Taylor length microscales |
| $\nu$ | fluid kinematic viscosity |
| $\rho$ | fluid density |
| $\sigma$ | mean square value of a Gaussian distribution |
| $\tau_w$ | average shear stress at the channel wall |
| $\tau_i$ | Lagrangian integral time scales |
| $\tau^*_{m,i}$ | time scale in Saffman's isotropic theory, equation (4) |
| $\tau_{m,i}$ | time scale in the non-isotropic extension of Saffman's theory, equation (11) |
| $\omega_i$ | RMS size of the fluctuating vorticity vector |
| $\omega_{rms,i}$ | $i$th component of the Eulerian RMS vorticity. |

at regular time intervals, time is a natural coordinate for monitoring the progress of the diffusion process. Averages for a fixed time involve a consideration of markers at different distances downstream of the source. In contrast, laboratory studies are usually made at a fixed distance away from the source and consider markers that have been in the field for different lengths of time. Since the theory of Lagrangian turbulent dispersion is formulated in terms of the diffusion time and no simple relation between downstream location of markers and time is available, comparisons of laboratory experiments with theory are complicated.

The influence of molecular diffusion on the property autocorrelation and, therefore, the turbulent diffusion coefficient is examined. Since the only available solidly based result is limited to small diffusion times, a goal of the present study is to provide an understanding of the effects of molecular diffusion for all times.

## 2. MOLECULAR DIFFUSIVITY EFFECTS AT SMALL TIMES

Saffman [3] showed that, in isotropic turbulence, the total dispersion at time $t$ in the $i$th direction, $D_i(t)$, can be expressed as

$$D_i(t) = 2\overline{u_i^2}\int_0^t (t-s)\cdot R_i(s)\,ds + 2\mathbf{D}\cdot t, \qquad (1)$$

if it is assumed that the markers are released at $t = 0$. Here, $D_i(t)$ is the mean-squared displacement of the diffusing marker, $\mathbf{D}$ is the molecular diffusion coefficient and $\overline{u_i^2}$ is the mean-square of the $i$th component of the fluctuating Eulerian velocity. The property autocorrelation, $R_i(s)$, at a given time delay, $s$, is defined as

$$R_i(s) \equiv \frac{\langle v_i(\mathbf{x}_0, 0)\cdot v_i(\mathbf{x}_0, s)\rangle}{\overline{u_i^2}}, \qquad (2)$$

where $v_i(\mathbf{x}_0, t)$ is the $i$th component of the fluctuating fluid velocity at the instantaneous position $\mathbf{X}(\mathbf{x}_0, t)$ of the marker which originated at $\mathbf{x}_0$ at the time of release. The usual convention that a repeated index indicates summation is not observed in this paper, unless otherwise stated. When the velocity products in (2) are computed along the trajectories of fluid particles, the standard Lagrangian autocorrelation, $R_{f,i}$, is recovered. It should be noted that in truly isotropic turbulence the indication of direction in (1) and (2) would have been redundant; this notation will be found convenient in channel flow, however, since it is necessary to distinguish among different directions.

Saffman [3] used the difference between the Lagrangian autocorrelation for fluid particles and the property autocorrelation as a measure of the interaction between molecular and turbulent diffusion. He found that, in isotropic turbulence, this difference is given, initially, as

$$R_{f,i}(s) - R_i(s) = s/\tau^*_{m,i}, \qquad (3)$$

where

$$\tau^*_{m,i} = \lambda_i^2/5\mathbf{D} \qquad (4)$$

where $\lambda_i$ is the Taylor length microscale.

Channel flow is inhomogeneous in the normal direction. At small times, however, most markers remain in the nearly homogeneous part of the flow in the center of the channel. Even in the center of the channel, nevertheless, the Eulerian flow shows significant anisotropy. At the conditions of the current flow simulation, the differences among the different components of the Eulerian turbulence intensities and RMS vorticities at the center ($u_{rms,1} = 0.812$, $u_{rms,2} = 0.589$, $u_{rms,3} = 0.599$ and $\omega_{rms,1} = 0.0425$, $\omega_{rms,2} = 0.0428$, $\omega_{rms,3} = 0.0487$) are non-negligible. These differences become larger with increasing distance from the centerline. The Taylor length microscales are often used as a criterion for isotropy. Lyons [14] has computed Taylor microscales for the flow conditions considered in the present paper. Table 1 presents these microscales, at the center of the channel, defined as

$$\lambda_{ij}^2 \equiv \overline{u_i^2}\Big/\overline{\left(\frac{\partial u_i}{\partial x_j}\right)^2}.$$

In exactly isotropic turbulence all the entries of Table 1 would be equal and any of the diagonal components of the microscale tensor could be used in equation (4).

Table 1. Eulerian Taylor length microscales at the center of the channel, made dimensionless with $u^*$ and $v$

| | | |
|---|---|---|
| $\lambda_{11} = 42.6$ | $\sqrt{2\lambda_{12}} = 30.6$ | $\sqrt{2\lambda_{13}} = 36.9$ |
| $\sqrt{2\lambda_{21}} = 37.5$ | $\lambda_{22} = 29.5$ | $\sqrt{2\lambda_{23}} = 31.8$ |
| $\sqrt{2\lambda_{31}} = 39.6$ | $\sqrt{2\lambda_{32}} = 30.4$ | $\lambda_{33} = 30.0$ |

The assumption of isotropy in Saffman's derivation can be easily relaxed. If attention is focused on small-time diffusion in the $i$th direction,

$$\langle v_i(\mathbf{x}_0, 0)\cdot v_i(\mathbf{x}_0, s)\rangle \approx \langle v_i(\mathbf{x}_0, 0)\cdot v_i(\mathbf{x}_0, s)\rangle_f + \mathbf{D}\cdot t\cdot\overline{u_i\nabla^2 u_i}. \qquad (5)$$

The term on the LHS of equation (5) is computed as an average of fluid velocity products along the trajectories of property particles; it depends on $Pr$. The subscript, f, on the bracketed term on the RHS of equation (5) indicates a quantity pertaining to fluid particles; it is, therefore, independent of $Pr$. It is also assumed in (5) that the average velocity in the $i$th direction is zero. The Eulerian turbulent term at the end of equation (5) arises from the interaction between molecular and turbulent diffusion; it can be rewritten as

$$\overline{u_i\nabla^2 u_i} = \overline{\nabla\cdot(u_i\nabla u_i)} - \overline{(\nabla u_i)^2}. \qquad (6)$$

The initial stages of the diffusion are dominated by small scales of motion which, in the center of the channel, can be assumed homogeneous. As a result, the 1st term on the RHS of equation (6) is approximately zero. The 2nd term can be expressed as

$$\overline{(\nabla u_i)^2} = \frac{\overline{u_i^2}}{\Lambda_i^2}, \qquad (7)$$

where $\Lambda_i$ is a length scale defined in terms of the Eulerian spatial Taylor microscales as

$$\frac{1}{\Lambda_i^2} = \frac{1}{\lambda_{i1}^2} + \frac{1}{\lambda_{i2}^2} + \frac{1}{\lambda_{i3}^2}. \qquad (8)$$

Both $\Lambda_i$ and $\overline{u_i^2}$ are computed at the center of the channel.

In inhomogeneous turbulence the particle velocity is expected to be represented by a nonstationary random process. Therefore, the definition of the property autocorrelation equation (2) should be renormalized as

$$R_i(s) \equiv \frac{\langle v_i(x_0, 0)\cdot v_i(\mathbf{x}_0, s)\rangle}{v_{rms,i}(0)\cdot v_{rms,i}(s)} \qquad (9)$$

in order for its interpretation not to be obscured by the effect of the varying magnitude of the turbulence intensities with time. The velocity products in equation (5) can be expressed in terms of the property autocorrelations by substituting equation (9) into (5).

The following equation is obtained if equations (6) and (7) are used:

$$R_{f,i}(s) - f_i(s) \cdot R_i(s) \approx f_{f,i} \cdot \frac{s}{(\tau_{m,i})}, \qquad (10)$$

where

$$f_i(s) \equiv \frac{v_{rms,i}(s)}{v_{f,rms,i}(s)} \quad f_{f,i}(s) \equiv \frac{v_{f,rms,i}(0)}{v_{f,rms,i}(s)} \quad \tau_{m,i} = \frac{\Lambda_i^2}{\mathbf{D}}. \qquad (11)$$

In deriving (10) use was made of the fact that the RMS Lagrangian velocity at $t = 0$ (for any $Pr$) is equal to the Eulerian turbulent RMS intensity at the center [i.e. $v_{rms,i}(0) = u_{rms,i}(y = 0)$]. If the flow in the center of the channel is assumed to be homogeneous and isotropic, equation (10) simplifies into equation (3).

The deviations of factors $f_i$ and $f_{f,i}$, introduced in equation (10), from unity reflect the flow inhomogeneities that the particles experience as they disperse into regions of varying Eulerian turbulence intensities. Factor $f_i$ deviates from unity because molecular diffusion causes the markers to disperse farther away from the centerline than the fluid particles which originate at the same positions. This effect is accentuated with decreasing $Pr$ number. Factor $f_{f,i}$ is independent of $Pr$ since it merely compares the intensity of the turbulence fluctuations at the centerline to those that the fluid particles sample, as they disperse towards the wall.

## 3. METHODS

### 3.1. *Direct numerical simulation of turbulent channel flow*

In order to calculate individual realizations of molecular paths, detailed instantaneous information about the flow is required. With a DNS of turbulence, the evolution of the fluctuating Eulerian velocity field at a large number of spatial locations is determined by solving the full three-dimensional time-dependent Navier–Stokes equations. Since the flow is directly calculated from first principles no modeliling is needed. Lyons *et al.* [1] have recently carried out a direct simulation of stationary, fully developed, turbulent flow in a two-dimensional channel at a low Reynolds number of 9048 based on the hydraulic diameter of the channel and the bulk streamwise velocity. Their code is employed in this work to supply instantaneous Eulerian velocity values.

The flow of an incompressible Newtonian fluid, driven by a constant mean pressure gradient, is considered. The velocity field is subject to periodic boundary conditions in the streamwise and spanwise directions, $x$ and $z$ respectively. The periodicity lengths, $L_x$ and $L_z$, determine the size of the computational domain in the corresponding directions. No-slip conditions are applied at the rigid channel walls which are separated by a distance $2H$. The Navier–Stokes equations are integrated in time using the pseudo-spectral fractional step method originally developed by Orszag and Kells [15] with the added correction suggested by Marcus [16] such that the proper boundary condition on the pressure field is enforced at the channel walls. All variables are made dimensionless with wall parameters, the kinematic viscosity, $v$, and the friction velocity, $u^* = \sqrt{(|\tau_w|/\rho)}$, where $\tau_w$ is the average shear stress at the wall and $\rho$ is the fluid density. Length, time, and pressure scales characteristic of the wall region are then constructed as $L^* = v/u^*$, $T^* = v/u^{*2}$, $P^* = \rho u^{*2}$.

The velocity field is represented as a truncated triple series of trigonometric functions in the homogeneous directions $x$ and $z$ and Chebyshev polynomials in the inhomogeneous normal direction. The use of Fourier series in the spanwise and streamwise directions satisfies the periodicity requirements in these directions automatically. The choice of a Chebyshev expansion in the direction normal to the channel walls naturally increases the spatial resolution of the computation in the high shear region close to the walls where steep gradients are expected.

The main input parameters for the flow simulation are the computational box dimensions, the number of grid points in each direction and the size of the time step. An initial velocity field is also required to start the computations. Results were obtained in a box of $L_x = 1900$, $2H = 300$ and $L_z = 950$ overlayed by a grid consisting of $128 \times 65 \times 128$ (in $x, y, z$ directions, respectively) grid points. The size of the time step was 0.25. Lyons *et al.* [1] determined that this time step value is sufficiently small for the Courant stability constraint to be satisfied. The channel code has been thoroughly validated in a thesis by Lyons [14] by comparisons with the experimental data of Niederschulte [17].

### 3.2. *Fluid particle tracking*

An algorithm for calculating trajectories of fluid particles in a DNS of a turbulent channel flow was recently described in a thesis by Kontomaris [18] and in a paper by Kontomaris *et al.* [2]. It is based on a numerical integration of the equation of particle motion; the position that a particle is initially assigned provides the initial condition for the integration. The integration is carried out with an explicit second-order Adams–Bashforth scheme, except for the first step where a second-order Runge–Kutta method is employed. A record of the random particle velocities and positions at selected sampling times is stored for statistical post-processing.

Let $\mathbf{x}(\mathbf{x}_0, t)$ and $\mathbf{V}(\mathbf{x}_0, t)$ denote the position and velocity at time $t$ of the fluid particle originating at $\mathbf{x}_0$ at time $t = 0$. The equation of motion for the particle is

$$\frac{d\mathbf{X}(\mathbf{x}_0, t)}{dt} = \mathbf{V}(\mathbf{x}_0, t) \qquad (12)$$

subject to the initial condition, $\mathbf{X}(\mathbf{x}_0, t=0) = \mathbf{x}_0$. The Lagrangian particle velocity $\mathbf{V}(\mathbf{x}_0, t)$ is related to the Eulerian velocity $\mathbf{U}$ by

$$\mathbf{V}(\mathbf{x}_0, t) = \mathbf{U}[\mathbf{X}(\mathbf{x}_0, t), t] \tag{13}$$

since the instantaneous particle velocity is the same as the fluid velocity at the particle position. From the DNS, the Eulerian velocity is available at each time step on a three-dimensional grid. Since the position of a particle does not, in general, coincide with a grid point, the particle velocity has to be evaluated by a three-dimensional interpolation of the Eulerian velocity grid point data. Accurate interpolation is required, since the Eulerian velocity fields vary sharply in space and numerical errors in the calculated particle trajectory can grow rapidly with time. Kontomaris *et al.* [2] evaluated particle velocities using a mixed spectral–polynomial interpolation scheme based on a Chebyshev series in the normal direction and Lagrange polynomials of degree 5 in the homogeneous directions of the channel. They demonstrated that such a scheme provides adequate accuracy for the purpose of extracting single-particle Lagrangian statistics without an excessive computational cost.

### 3.3. *Stochastic modelling of molecular diffusion*

The molecular diffusion process is usually visualized as the spreading of a substance from a region of high concentration to one of lower concentration, i.e. down a concentration gradient. This spreading is the net result of the erratic motion of the molecules of the diffusing substance. This spreading is the net result of the erratic motion of the molecules of the diffusing substance. In this paper, molecular diffusion is modelled in a statistical sense by the extensively studied class of stochastic processes known as "Random Walks". As Egan [19] observes, in the case of a three-dimensional random walk, the probability of a marker, from a group of markers enclosed in a sphere, crossing the boundary of the sphere and migrating into the unpopulated region outside the sphere is non-zero. The probability of the reverse process, however, is zero since no markers exist outside the sphere. Therefore, the markers on average move from high to low concentration regions, which is consistent with the usual concept of a diffusion process.

The mathematical and physical ramifications of the random walk (or random flights) problem have been reviewed in detail by Chandrasekhar [20]. He pointed out that the motion of a large number of particles executing random flights in a three-dimensional space without mutual interference can be interpreted as a diffusion process with a diffusion coefficient related to the mean square displacement of the particles which is to be expected at each step. The well-known random vortex method for solving the vorticity transport equation uses a random walk approach to simulate the molecular diffusion of vorticity blobs [19, 21]. The concept of a random walk was also employed by Drummond *et al.* [12] and by Sawford and Hunt [13] in order to incorporate molecular diffusion effects into their Lagrangian models of turbulent diffusion.

Chandrasekhar [20] studied the problem of a particle undergoing a sequence of random displacements, for which the magnitude and direction of each is independent of all the preceding ones. For an uncorrelated (and therefore independent) three-dimensional joint Gaussian distribution of the displacements, the diffusion coefficient in an isotropic medium and the mean square displacement in each direction over a single step are related as

$$\sigma_{x_i}^2 = \sigma_{i_i}^2 = \sigma_{z_i}^2 = \sigma_m^2 = 2\mathbf{D}t. \tag{14}$$

In terms of quantities measured in wall units, the above equation is rewritten as

$$\sigma_m = \sqrt{\left(\frac{2}{Pr}\Delta t_{tr}\right)}, \tag{15}$$

where $Pr = \nu/\mathbf{D}$ is the Prandtl number and $\nu$ is the kinematic viscosity of the fluid. The molecular diffusion mechanism was incorporated in the fluid particle tracking algorithm of Kontomaris [18] by dividing the instantaneous displacement $\Delta\mathbf{X}(\mathbf{x}_0, t)$ of a marked molecule into two separate components: a hydrodynamic component $\Delta\mathbf{X}_h(\mathbf{x}_0, t)$ which was determined by the convective motion of the fluid particle containing the molecule at a given instant and a molecular component $\Delta\mathbf{X}_m(\mathbf{x}_0, t)$ determined by the random molecular motion,

$$\Delta\mathbf{X}(\mathbf{x}_0, t) = \Delta\mathbf{X}_h(x_0, t) + \Delta\mathbf{X}_m(\mathbf{x}_0, t). \tag{16}$$

The two contributions are treated as independent and additive due to the large difference in the scales of molecular and turbulent motion. The contribution of the turbulent motion, $\Delta\mathbf{X}_h$, is computed from equation (12). The random molecular increments, $\Delta\mathbf{X}_m$, are chosen to be normally distributed and mutually independent in the three different coordinate directions:

$$\Delta\mathbf{x}_m(\mathbf{x}_0, t) = \sigma_m \cdot \mathbf{W}, \tag{17}$$

where $\mathbf{W}$ stands for three independent standard Gaussian random numbers with zero mean and variance $\sigma^2 = 1$. They are also independent from one molecule to another (so that there is no molecule-to-molecule interaction) and from time step to time step (so that the progress of the molecular motion does not depend on the earlier history of the molecular path). In the case that a particle reaches and penetrates a channel wall, thus being brought outside of the computational domain, it is reflected symmetrically back into the channel. This is equivalent to enforcing the boundary condition of an adiabatic or impermeable wall [20].

### 3.4. *Details of implementation*

For an accurate integration of [12] the time step size $\Delta t_{tr}$ has to be restricted to sufficiently small values. As a rule, the smaller the displacement in a single time step the more accurate the integration. As a sufficient

constraint on the time step for an accurate computation of molecular trajectories, it is required that the total typical displacement of a molecule (from [16]) in any direction over a single time step does not exceed an appropriate small length scale. If the grid spacing in the respective direction in the center of the channel is selected as such a scale, it is found that a time step of $\Delta t_{tr} = 0.25$ is sufficiently small for even the smallest Prandtl number (which gives rise to the largest molecular jumps) examined in this study. The sufficiency of this condition to produce Lagrangian statistics independent of the time step was tested with a low resolution simulation in a small computational box of dimensions $L_x = 630$, $2H = 250$ and $L_z = 630$ and a grid of $16 \times 33 \times 64$ (in $x, y, z$ directions, respectively) points. The tracking time step was varied in the range permitted by the above condition and it was confirmed that it had no effect on the computed results.

A large number (16 129) of molecules were released simultaneously at time $t = t_0$ and assigned initial positions that spread them over a horizontal $xz$-plane at the center of the channel (i.e. $y = 0$). The initial positions of the molecules form a mesh with uniform spacings $\Delta x_{pr} = 14.921$ and $\Delta z_{pr} = 7.422$. Their trajectories are then traced for a total time sufficiently long for the fluid velocity at the position of the molecules to become uncorrelated with its initial value at the time of release. The statistical homogeneity of the Eulerian fields in the streamwise and spanwise directions removes any statistical dependence on the $x$ and $z$ coordinates of the source location. Therefore, ensemble averaging over molecules released at different $x$ and $z$ locations is permitted. Similarly, the stationarity of the Eulerian fields renders the time of release $t_0$ irrelevant, thus justifying, if necessary, ensemble averaging over molecules released at different times, too. The number of molecules allocated was restricted by the number of grid points over a horizontal plane needed to resolve the Eulerian fields. The molecules are released at positions about one grid spacing apart; releasing more molecules would not improve the statistical sample (except perhaps at long diffusion times) because the motion of adjacent particles would be, initially, strongly correlated. Five tracking experiments are performed in the same turbulence simulation for computational economy. Prandtl or Schmidt numbers equal to 0.05, 0.1, 0.5 and 1.0 were studied, for which the RMS jump sizes (in one time step of 0.25 wall units) from [15] are 3.162, 2.236, 1.000 and 0.707, respectively. The case of fluid particles, which can be viewed as a limit of molecules with an infinite Prandtl number, was also included in this study as a basis from which to assess molecular diffusivity effects.

The next section presents a Lagrangian statistical description of the dispersion of molecules of different Prandtl numbers originating at the center of the channel under the synergistic action of both turbulent and molecular diffusion. Clearly the property autocorrelation is the key quantity of interest; other statistical quantities are also reported in order to provide a more complete picture of the dispersion and to facilitate the interpretation of the property autocorrelations. Fair statistical sampling requires averaging over many independent realizations of particle trajectories and many independent turbulence realizations. The statistical error, because of the use of an ensemble consisting of a necessarily finite number of molecular trajectories, deteriorates at longer diffusion times and larger molecular diffusivities (or smaller Prandtl numbers) because the molecules spread out and occupy a larger amount of space. Statistical convergence was judged by comparing the computed statistics to statistics averaged over only half (i.e. 8064) of the available trajectory realizations. It was found that the reported statistics were free of significant statistical error. The dependence of the computed statistics on the peculiarities of the turbulence at the instant of release is expected to be insignificant because of the large size of the computational box. This dependence also weakens with decreasing Prandtl number because molecules of high molecular diffusivity follow less closely the organized turbulent structures that might exist in the center of the channel at the time of release.

## 4. RESULTS

The motion of a single particle is described completely by the vector function $\mathbf{X}(\mathbf{x}_0, t)$ which gives the position of the particle at any time $t$. The trajectories of two discrete molecules with $Pr = 0.1$ and $Pr = 1$ and the fluid particle in which they were originally placed are compared in Fig. 1, where only the side view is shown. All particles are released simultaneously at the point $(x = 0, y = 0, z = 7.42)$ and their trajectories are computed for a total time of 123.5 wall units. The trends of all three trajectories are similar since they are all determined by approximately the same hydrodynamics (at least for as long as the deviations remain small).

In place of the position vector, $\mathbf{X}(\mathbf{x}_0, t)$, one may use the particle displacement vector during the time interval $t$:

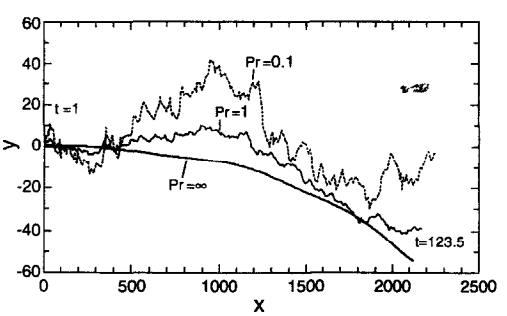


FIG. 1. Comparison of the trajectories of two molecules with $Pr = 0.1$ and 1.0 and of the fluid particle in which they were released, at the center of the channel and traced for 123.5 wall time units.

$$\mathbf{Y}(t) = \mathbf{X}(\mathbf{x}_0, t) - \mathbf{x}_0 = \int_0^t \mathbf{V}(\mathbf{x}_0, t)\,\mathrm{d}t. \qquad (18)$$

In order to consider the statistical characteristics of the displacement fluctuations it is necessary to subtract the mean value of the displacement vector, $\langle \mathbf{Y} \rangle$, to obtain

$$\mathbf{Y}'(\mathbf{x}_0, t) = \mathbf{Y}(\mathbf{x}_0, t) - \langle \mathbf{Y}(t) \rangle, \qquad (19)$$

where $\langle\ \rangle$ indicates averaging over the parameter $\mathbf{x}_0$, i.e. over all particles. Statistics of particle position (or displacement) are related to particle velocity statistics through equation (18) and, to statistics of the Eulerian velocity field through equation (13). The focus of this section is the description of the statistical characteristics of the particle velocity ($V_1(t)$, $V_2(t)$, $V_3(t)$) and displacement ($Y_1(t)$, $Y_2(t)$, $Y_3(t)$) vectors. All results are scaled with wall parameters.

### 4.1. *Displacement distributions*

The three-dimensional probability density of $\mathbf{Y}$, $p(\mathbf{y} \mid t;\ Pr)$, depends on the diffusion time $t$ and $Pr$. The function $p(\mathbf{y} \mid t;\ Pr)$ may also be interpreted as the mean volumetric concentration $\bar{C}(x_1, x_2, x_3, t)$ field resulting from an instantaneous point source of unit concentration at the origin (0, 0, 0) at the initial $t_0 = 0$. The number of independent variables can be reduced by integrating the function $\bar{C}(x_1,\ x_2,\ x_3,\ t)$ over all values of $x_1$ and $x_3$. The resulting function, $p(y_2 \mid t;\ Pr)$, describes the one-dimensional distribution.

Figure 2 shows the displacement distribution across the channel at a dimensionless diffusion time of 50 for different $Pr$. These curves were computed according to the definition of a probability density function:

$$p(y_2 \mid t; Pr) = \lim_{\Delta y_2 \to 0} \left[ \frac{P(y_2 \leqslant Y_2(t) < y_2 + \Delta y_2)}{\Delta y_2} \right] \qquad (20)$$

where

$$P = \frac{\text{number of particles with } y_2 \leqslant Y_2(t) < y_2 + \Delta y_2}{\text{total number of particles}}. \qquad (21)$$

According to the above definition

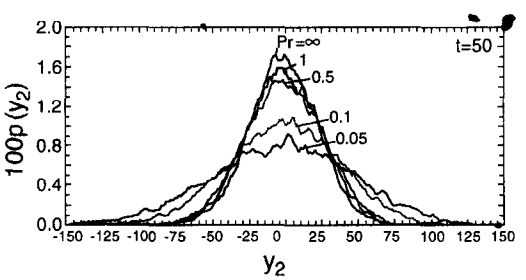


FIG. 2. Probability density of the normal coordinate of property particles with different $Pr$ numbers at a moderate diffusion time ($t = 50$).

$$\int_{-H}^{H} p\,\mathrm{d}y_2 = 1. \qquad (22)$$

At any given time the range of $y_2$ values over which particles are found is divided into a number of bins and the particles with a normal coordinate falling within each bin are counted. The bin width, $\Delta y_2$, is chosen sufficiently small to resolve the variation in the computed distributions but large enough to smooth out unwanted statistical noise.

It is seen in Fig. 2 that within 50 wall time units, molecules with $Pr = 0.05$ start reaching the channel walls. After 100 time units markers of all $Pr$ numbers examined reach the channel walls. The shapes of the distributions were found to obey (approximately) the following expression:

$$p(y_2 \mid t; Pr) = \bar{C}_{\max}(t; Pr) \cdot \exp\left[ -\frac{y_2^2}{2\sigma_2^2(t; Pr)} \right]. \qquad (23)$$

The (decaying) maximum concentration, $\bar{C}_{\max}$, occurs at the centerline. The values of $\bar{C}_{\max}$, $\sigma_2$ which minimize the mean-square deviations between the predictions from (23) and the actually computed curves in Fig. 2 are given in Table 2. The correlation coefficient, $R$, included in Table 2, is a measure of the goodness of the fit; the square of $R$ represents the proportion of the observed variation which can be accounted for by the regression curve [22]. For equation (23) to represent a Gaussian distribution, the two regression parameters $\bar{C}_{\max}$ and $\sigma_2$ must satisfy the condition

$$\bar{C}_{\max} \cdot \sigma_2 \cdot \sqrt{(2\pi)} \approx 1. \qquad (24)$$

Observed values of $\bar{C}_{\max} \cdot \sigma_2 \cdot \sqrt{(2\pi)}$ are also tabulated in Table 2.

### 4.2. *Mean velocity*

The time-history of the mean particle velocity determines the mean downstream displacement of the center of gravity of a contaminant cloud with respect to the position of the source. The computed mean streamwise particle velocity for different Prandtl numbers is shown in Fig. 3. It is the result of the sampling by the particle of the Eulerian streamwise velocity field at different positions across the channel cross-section. Its initial value is equal to the Eulerian mean velocity at the centerline, $\mathbf{U}_c$, obtained as an instantaneous average over the horizontal directions at the time of release. Surprisingly, it increases initially. This is counterintuitive because, as the particles spread away from the centerline, their average velocity would have been expected to follow the decreasing trend of the Eulerian mean velocity. This phenomenon, which becomes less pronounced as the Prandtl number decreases, is due to biased sampling of the Eulerian fields. Fluid particles in the center represent aging turbulence whose mean velocity tends to increase

Table 2. Best estimated values for the regression parameters, $\bar{C}_{max}$ and $\sigma_2$, in equation (23) used to approximate the computed displacement distributions in Fig. 2

| $Pr$ | $100\bar{C}_{max}$ | $\sigma_2$ | $R^2$ | $\bar{C}_{max} \cdot \sigma_2 \cdot \sqrt{(2\pi)}$ |
|---|---|---|---|---|
| $\infty$ | 1.5565 | 24.49 | 0.956 | 0.96 |
| 1 | 1.5697 | 25.38 | 0.98 | 1.00 |
| 0.5 | 1.5279 | 26.51 | 0.97 | 1.02 |
| 0.1 | 1.022 | 38.3 | 0.958 | 0.98 |
| 0.05 | 0.80391 | 49.07 | 0.953 | 0.99 |

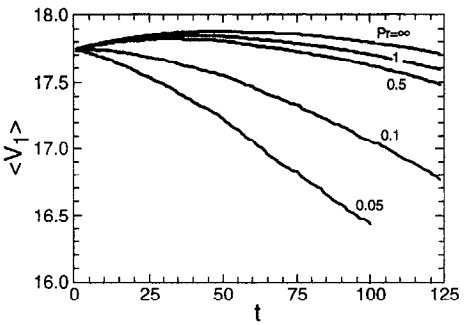


FIG. 3. Average streamwise particle velocity.

because of the action of the mean pressure gradient [18].

### 4.3. *RMS particle velocities*

The fluctuating particle velocity, $\mathbf{v}(\mathbf{x}_0, t)$, (defined as $\mathbf{V}(\mathbf{x}_0, t) - \langle \mathbf{V} \rangle$) is nonstationary initially due to the inhomogeneities of the flow in the normal direction. At long times it is expected to become stationary as a result of the boundedness of the flow in the inhomogeneous direction. The root-mean-square fluctuating particle velocities, $v_{rms,i}$, are shown in Fig. 4. It is seen that they initially decrease with time even at small times when most of the particles are in a region where the Eulerian intensities are either constant or slightly increasing. This phenomenon, which becomes less pronounced at low $Pr$, is consistent with the observed increase in the mean velocity discussed above. At long times the RMS particle velocities increase because the particles penetrate into regions of higher turbulence intensities as they approach the wall. The effect of wall inhomogeneities is manifested earlier in the lower $Pr$ particles because, for any given time, they travel farther away from the center.

The inhomogeneity factors, $f_i$ and $f_{f,i}$, introduced in Section 2 can be easily calculated from the curves in Fig. 4. At small times they remain close to their homogeneous value of unity. At $t = 10$, for example, $f_{f,1} = 1.063$, $f_{f,2} = 1.041$ and $f_{f,3} = 1.017$; at the same time ($t = 10$), $f_1 = 1.086$, $f_2 = 1.03$ and $f_3 = 1.027$ for $Pr = 0.05$.

### 4.4. *Dispersion*

The mean square value of the fluctuations of the total (i.e. including both molecular and turbulent) displacement, $D_i(t) = \langle Y_i^2(\mathbf{x}_0, t) \rangle$, is usually referred

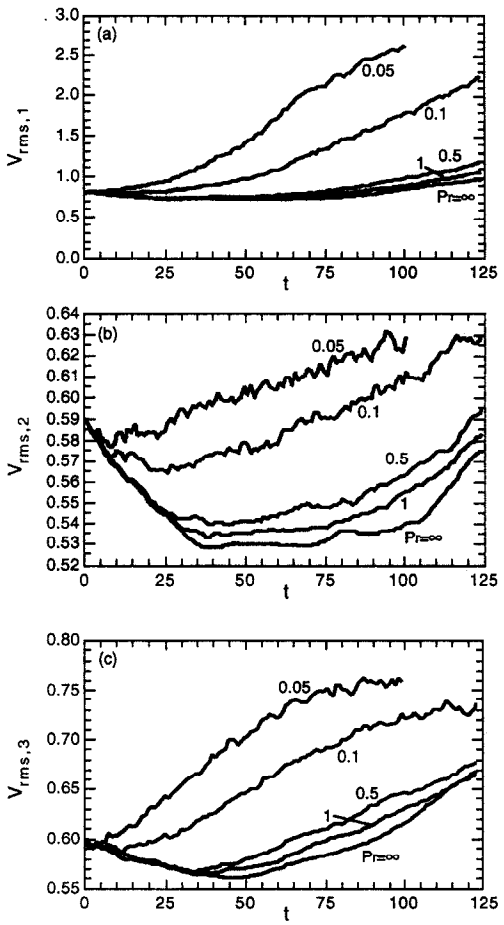


FIG. 4. Root-mean-square fluctuating particle velocities.

to as the dispersion. The cloud of contaminated particles spreads around its center of gravity as it is convected downstream; its average linear dimension at any time instant, $t$, is proportional to $[D_1(t) \cdot D_2(t) \cdot D_3(t)]^{(1/3)}$. At small times and low $Pr$, the dispersion is dominated by molecular diffusion, so it increases linearly at a rate roughly equal to $2/Pr$. The square roots of directly computed values of the total dispersions corresponding to the displacement distributions of Fig. 2 are in good agreement with the values of $\sigma_2$ (given in Table 2) used to fit the displacement distributions.

The total displacements in the homogeneous direc-

tions are nonstationary because the particles continue to spread without limit. The normal component of the dispersion, however, is limited by the presence of the walls and has to approach a constant value corresponding to a uniform distribution across the channel. At this asymptotic limit the probability density of the displacement becomes equal to $1/2H$ and its second moment reaches a value of

$$D_{2,\max} = \frac{(2H)^2}{12} = \frac{(2 \cdot 150)^2}{12} = 7500.$$

The convective contributions to the dispersion, calculated as $D_i(t) - 2t/Pr$, are shown in Fig. 5. The only convective contribution in the transverse directions is due to the turbulence. In the streamwise direction, however, the varying velocity also enhances the dispersion [23–25]. The effect is manifested at times sufficiently large for the dispersing particles to experience appreciable mean velocity gradients. For small diffusion times, turbulence remains the dominant contributor to the dispersion in all three flow directions.

For small times, turbulent dispersion depends primarily on the intensity of turbulent velocity fluctuations. This is illustrated by the initial independence of the dispersion curves in Fig. 5 of $Pr$. Although the total dispersion increases with decreasing $Pr$, the turbulent contribution to the dispersion in the transverse directions, Figs. 5(b), 5(c), exhibits a reverse trend. This is because the effective length scale of the eddies which disperse the property particles diminishes with decreasing $Pr$ (or increasing molecular diffusivity) as a result of the added decorrelating effect of molecular diffusion. This effect can be visualized as associated with "leaky eddies"; markers leak in random directions along the coherent path of an eddy because of molecular diffusivity, thereby reducing the dispersive effectiveness of the turbulence.

It is notable that, in the normal direction, the turbulence contribution to the dispersion for particles with $Pr = 0.05$ reaches a maximum at approximately $t \approx 85$. The total dispersion at that time is

$$D_2(t \approx 85; Pr = 0.05) = \left(D_2 - \frac{2t}{Pr}\right) + \frac{2t}{Pr} \approx 600 + \frac{2 \times 85}{0.05} = 4000$$

or only 53% of the maximum allowable. The total dispersion curve (shown in the thesis of Kontomaris) for $Pr = 0.05$ exhibits a S-shaped variation which, superficially, resembles the experimental dispersion curve observed by Vames and Hanratty [26] for the case of droplets traced for long times.

In the streamwise direction (Fig. 5a) molecular diffusion enhances turbulent dispersion because the added dispersive contribution associated with the varying mean velocity can offset the effect associated with "leaky eddies". This enhanced streamwise dispersion is more prominent at low $Pr$ because the particles disperse over larger distances from the centerline (for a given diffusion time) and therefore experience a greater variation in the streamwise mean velocity.

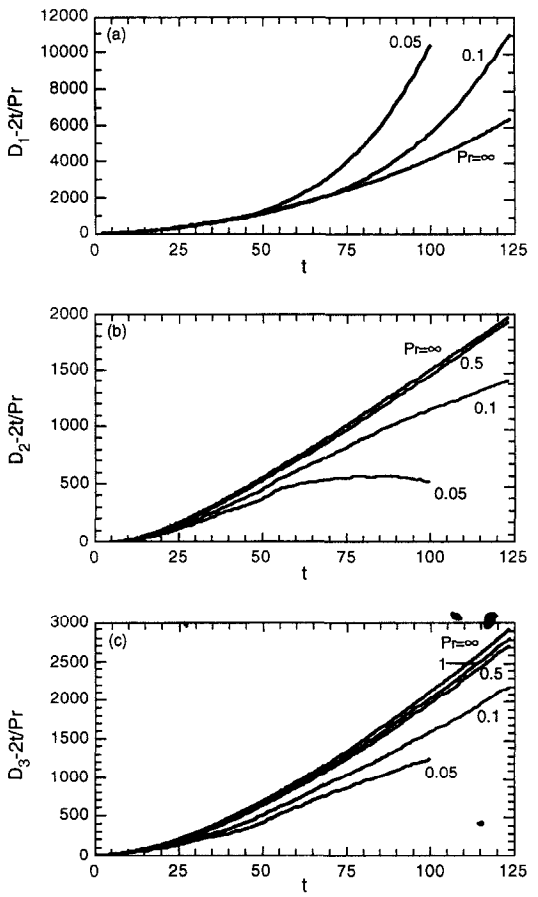


FIG. 5. Convective contributions to the mean-square particle dispersion.

### 4.5. *Property autocorrelations*

The influence of $Pr$ on the property autocorrelations, calculated from equation (9), is shown in Fig. 6. The curves for $Pr = 1$ and 0.5 are close to that for a fluid particle, $Pr = \infty$. However, molecular diffusion is found to have a strong effect on the property autocorrelation for $Pr = 0.1$ and 0.05. The initial shape of the property autocorrelations gradually changes from parabolic to linear as the $Pr$ decreases. At long times the normal autocorrelation assumes negative values as a result of outflows from the wall region. Such negative tails were more clearly apparent in autocorrelations computed by the low resolution simulation mentioned in Section 3.1, which was extended to times up to 250 wall units. It is also interesting to note that the Lagrangian statistics become more isotropic as $Pr$ decreases. The computed property autocorrelations for $Pr = 0.05$ are the same in all three directions despite the significant anistropy exhibited in the curves for $Pr = \infty$.

Lagrangian integral time scales of the normal and spanwise velocity components of the particle, defined as $\tau_i = \int_0^\infty R_i(s)\,ds$ are presented in Table 3. Figure

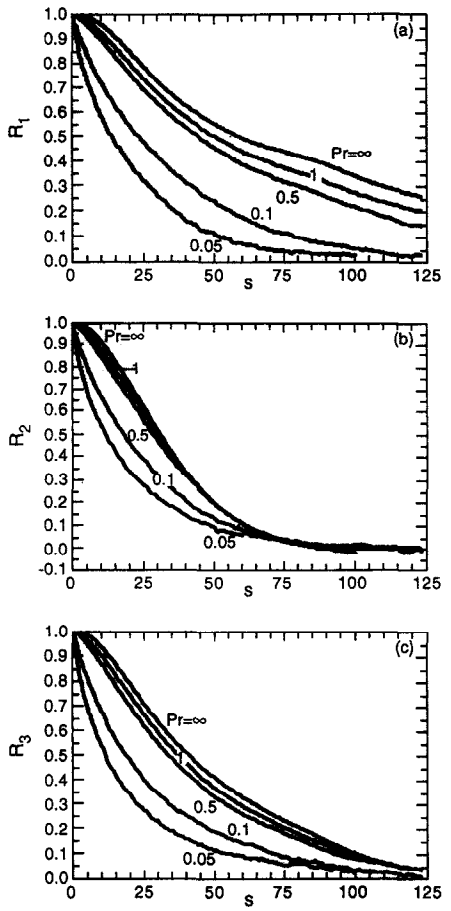


FIG. 6. Effect of $Pr$ on the computed property autocorrelation.

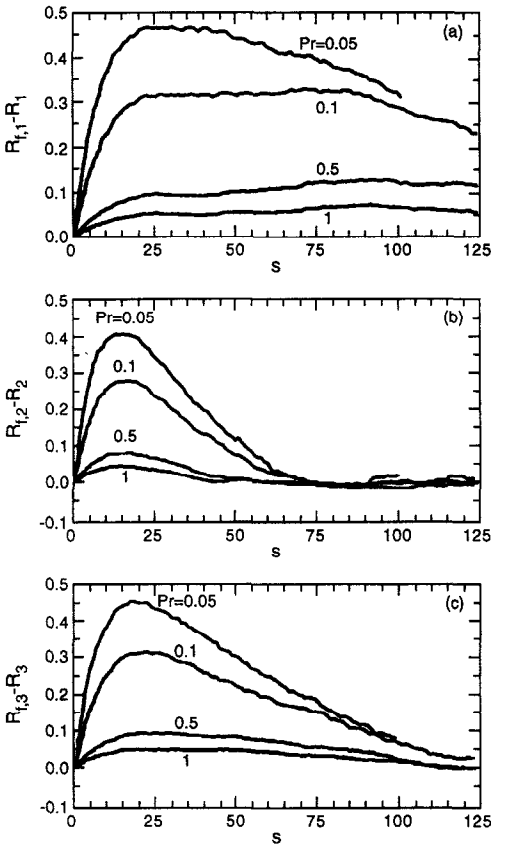


FIG. 7. Effect of $Pr$ on the difference between the fluid and the property autocorrelation.

6(c) shows that the total tracking time was not sufficient for the spanwise autocorrelations to drop to zero. The spanwise integral scales were computed by fitting the computed $R_3$ curves with an exponential function and extrapolating to times where they became negligible. The contributions from the extrapolated tails of the correlations were no more than 3.5%. A rapid decrease of the time scale with decreasing $Pr$ is observed at low Prandtl numbers. It should be pointed out that the choice of an appropriate velocity scale for the conversion of these integral time scales into eddy diffusivities is not obvious because the flow is inhomogeneous.

Table 3. Lagrangian integral time scales of the normal and spanwise property autocorrelations

| $Pr$ | $\tau_2$ | $\tau_3$ |
|---|---|---|
| 0.05 | 19.2 | 21.9 |
| 0.1 | 24.3 | 29.7 |
| 0.5 | 31.9 | 45.3 |
| 1 | 33.6 | 48.3 |
| $\infty$ | 33.8 | 52.0 |

## 5. DISCUSSION

It would be convenient if the shape of the property autocorrelation could be described by some simple function. The autocorrelations for $Pr = 0.1$ are very close to an exponential in all three directions. However, no general conclusion can be drawn regarding the agreement of the computed correlations with an exponential function. The complicated shape of the correlations can be, partially, attributed to the fact that different portions of the curves, for different times and different $Pr$, are determined by different turbulence hydrodynamics because of the inhomogeneity of the flow. An additional complication results because the transitional value of the $Re$ used in the simulation precludes a behavior characteristic of either a high or a low $Re$ asymptotic limit.

### 5.1. *Behavior at large times*

Saffman [3] speculated that, for homogeneous turbulence and sufficiently high $Re$, the normalized difference $[R_{f,i}(s) - R_i(s)]/R_{f,i}(s)$ should become independent of time delay, $s$, at long times. The theoretical calculations of Kontomaris and Hanratty [7] support this notion. The maxima exhibited by the plots of $[R_{f,i}(s) - R_i(s)]$ in Fig. 7 are consistent with these

results. The difference can be viewed as the product of $[R_{f,i}(s)-R_i(s)]/R_{f,i}(s)$ and $R_{f,i}(s)$. The latter two quantities exhibit opposite trends with time and, as a result, their product exhibits a maximum. These maxima decrease and become broader with increasing $Pr$.

The results in Fig. 7 and the values of $R_i$ in Fig. 6 for $Pr = \infty$ are used to develop the plot in Fig. 8. The rate of change of $[R_{f,i}(s)-R_i(s)]/R_{f,i}(s)$ diminishes with time. A constant asymptotic value of this ratio was not reached in the streamwise direction within the tracking time covered. In the normal direction, due to the smaller characteristic time scales, a long time behavior is approached within times sufficiently small that most particles still remain in the nearly homogeneous part of the flow in the center of the channel. Consequently, the ratios $[R_{f,2}(s)-R_2(s)]/R_{f,2}(s)$ approach values which remain approximately constant for some time. These asymptotic values are reached earlier for higher $Pr$; their magnitude increases toward unity with decreasing $Pr$. Both of these observations are in qualitative agreement with the isotropic turbulence calculations of Kontomaris and Hanratty [7]. At longer times, however, the ratio $[R_{f,2}(s)-R_2(s)]/R_{f,2}(s)$ decreases because of the influence of flow inhomogeneities. At even longer times both $R_{f,2}$ and $R_2$ approach zero and statistical and numerical uncertainty do not permit an accurate determination of the above ratio.

### 5.2. *Behavior at small times*

The difference $[R_{f,1}(s)-R_1(s)]$ is convenient for quantifying molecular diffusivity effects at small times. The small time portion of the curves in Fig. 7 can be interpreted by the generalization of Saffman's small time theory, equation (10), presented in Section 2. The characteristic time scale for the interaction between molecular and turbulent diffusion, $\tau_{m,1}$, in wall units is obtained by rescaling, equation (11c), with wall parameters, $\tau_{m,1} = Pr\,\Lambda_1^2$. Values of $\Lambda_i$ ($\Lambda_1 = 15.5$, $\Lambda_2 = \Lambda_3 = 14.8$) are calculated from equation (8) with Taylor microscales from Table 1. The corrections represented by factors $f_1$ and $f_{f,i}$ make only a small contribution because they remain very close to unity for the small times that Saffman's theory is applicable.

Figure 9 examines the agreement between the computed autocorrelation differences and equation (10), which is represented by the dashed lines going through the origin. The agreement is satisfactory at small times. The range of validity of equation (10) is more limited in the streamwise direction than in the two transverse directions, probably because of the varying mean streamwise velocity which is not accounted for

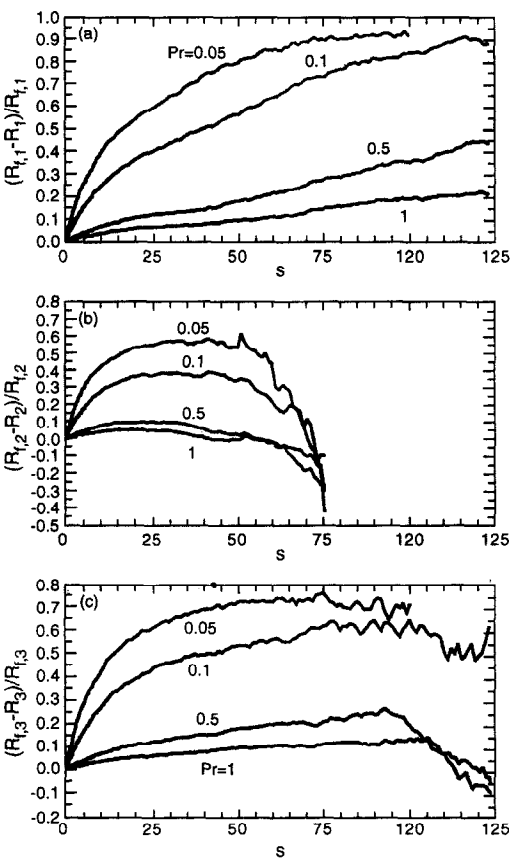


FIG. 8. Normalized values of the difference of the fluid and property autocorrelations.

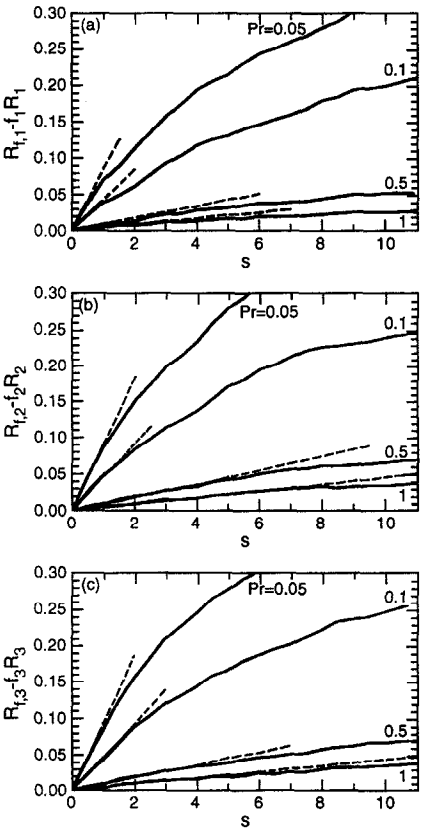


FIG. 9. Comparison of the small time behavior of the difference of the fluid and the property autocorrelation with a generalization of Saffman's theory for anisotropic turbulence.

in the derivation of (10). In addition, the streamwise Eulerian intensity increases more rapidly with distance from the centerline than do the two transverse components [14]. In all three directions, the range of validity of equation (10) narrows with decreasing $Pr$. This is a consequence of the inherent limitation in Saffman's derivation, equation (6), imposed by the assumption that the size of the diffusing property element be small compared to the length scale of the rotational and straining motions of the turbulence. The time scale of the turbulence motions at the channel center [which can be estimated as $1/\omega = 12.9$ with $\omega = \sqrt{(\bar{\omega}_i \cdot \bar{\omega}_i)}$ (summation on $i$) being the RMS size of the fluctuating vorticity vector] places an upper bound to the times at which (10) can be expected to be a reasonable approximation. It should be noted, however, that the agreement between the computed data and Saffman's strictly isotropic result in equation (3) [using the Taylor length microscales, $\lambda_i$, from Table 1 in equation (4)] is limited to a more narrow range of times than equation (10), especially in the streamwise direction.

## 6. CONCLUSIONS

The effect of molecular diffusivity on turbulent diffusion from a point source of heat or mass was investigated by computing molecular trajectories in the center of a direct numerical simulation of channel flow. The fluid velocity along the trajectory of a heat or mass element and its displacement from the location of the source are described in terms of 1st and 2nd order statistics.

The shape of the property autocorrelations changes drastically with Prandtl number and it cannot be described by a simple exponential or Gaussian function. The effect of Prandtl number for small diffusion times is accurately described by Saffman's theory, generalized for anisotropic turbulence. For long diffusion times, the computed autocorrelations suggest that in homogeneous turbulence the ratio $[R_{f,i}(s) - R_i(s)]/R_{f,i}(s)$ approaches a value independent of $s$. This constant value approaches unity in the limit of small Prandtl numbers.

*Acknowledgements*—This work was supported by the National Science Foundation under contract NSF CTS-92-09877. The support and facilities of the National Center for Supercomputing Applications at the University of Illinois, Urbana is also acknowledged.

## REFERENCES

1. S. L. Lyons, T. J. Hanratty and J. B. McLaughlin, Large-scale computer simulation of fully developed turbulent channel flow with heat transfer, *Int. J. Numer. Methods Fluids* **13,** 999–1026 (1991).
2. K. Kontomaris, T. J. Hanratty and J. B. McLaughlin, An algorithm for tracking fluid particles in a spectral simulation of turbulent channel flow, *J. Comp. Phys.* **103** (2), 231–242 (1992).
3. P. G. Saffman, On the effect of the molecular diffusivity in turbulent diffusion, *J. Fluid Mech.* **8,** 273–283 (1960).
4. P. G. Saffman, Some aspects of the molecular diffusivity in turbulent diffusion, *Mécanique de la turbulence* (*Coll. Intern. du CNRS à Marseille*), Paris, Éd. CNRS, pp. 53–62 (1962).
5. G. I. Taylor, Diffusion by continuous movements, *Proc. Lond. Math. Soc. Ser.* 2 **A20,** 196–211 (1921).
6. J. O. Hinze, *Turbulence*. McGraw-Hill, New York (1959).
7. K. Kontomaris and T. J. Hanratty, Effect of molecular diffusivity on turbulent diffusion in isotropic turbulence, *Int. J. Heat Mass Transfer* **36,** 1403–1412 (1993).
8. S. Corrsin, Progress report on some turbulent diffusion research, *Adv. Geophys.* **6,** 161–164 (1959).
9. S. Corrsin, Theories of turbulent dispersion, *Mécanique de la turbulence* (*Coll. Intern. du CNRS à Marseille*), Paris, Éd. CNRS, pp. 27–52 (1962).
10. R. Phythian and W. D. Curtis, The effect of long-time diffusivity for a passive scalar field in a Gaussian model fluid flow, *J. Fluid Mech.* **89,** 241–250 (1978).
11. I. T. Drummond, Path-integral methods for turbulent diffusion, *J. Fluid Mech.* **123,** 59–68 (1982).
12. I. T. Drummond, S. Duane and R. R. Horgan, Scalar diffusion in simulated helical turbulence with molecular diffusivity. *J. Fluid Mech.* **138.** 75–91 (1984).
13. B. L. Sawford and J. R. C. Hunt, Effects of turbulence structure, molecular diffusion and source size on scalar fluctuations in homogeneous turbulence, *J. Fluid Mech.* **165,** 373–400 (1986).
14. L. S. Lyons, A direct numerical simulation of fully developed turbulent channel flow with passive heat transfer, Ph.D. Thesis, University of Illinois, Urbana, IL (1989).
15. S. A. Orszag and L. C. Kells, Transition to turbulence in plane Poiseuille and plane Couette flow, *J. Fluid Mech.* **96,** 159–205 (1980).
16. P. S. Marcus, Simulation of Taylor–Couette flow, *J. Fluid Mech.* **146,** 45 (1984).
17. M. A. Niederschulte, Turbulent flow through a rectangular channel, Ph.D. Thesis, University of Illinois, Urbana, IL (1989).
18. K. Kontomaris, Point source dispersion in a numerically simulated turbulent channel flow, Ph.D. Thesis, University of Illinois, Urbana, IL (1991).
19. E. W. Egan, Computational simulation of buoyancy-driven flows using vortex methods, Ph.D. Thesis, University of Illinois, Urbana, IL (1989).
20. S. Chandrasekhar, Stochastic Problems in Physics and Astronomy, *Rev. of Modern Physics* **15,** No. 1 (1943).
21. A. J. Chorin, Numerical study of slightly viscous flow, *J. Fluid Mech.* **57,** 785–796 (1973).
22. R. H. Myers, *Classical and Modern Regression with Applications*, p. 30. Duxbury Press (1986).
23. G. I. Taylor, Dispersion of soluble matter in solvent flowing slowly through a tube, *Proc. R. Soc. Lond. Ser. A* **219,** 186–203 (1953).
24. G. I. Taylor, The dispersion of matter in turbulent flow through a pipe, *Proc. R. Soc. Lond. Ser. A* **223,** 446–468 (1954a).
25. G. I. Taylor, Conditions under which dispersion of a solute in a stream of solvent can be used to measure molecular diffusion, *Proc. R. Soc. Lond. Ser. A* **225,** 473–477 (1954b).
26. J. S. Vames and T. J. Hanratty, Turbulent dispersion of droplets for air flow in a pipe, *Exper. Fluids* **6,** 94–104 (1988).